Aerotecnica Missili & Spazio (2025) 104:247–256
https://doi.org/10.1007/s42496-024-00228-2

RESEARCH

Material Characterisation of Deflated Structured Fabrics

E. Rustighi[1] · P. Gardonio[2] · S. Baldini[2] · C. Malacarne[3] · M. Perini[3]

Received: 27 March 2024 / Revised: 17 June 2024 / Accepted: 19 June 2024 / Published online: 2 July 2024

Abstract
Structured fabrics are made by interwoven rigid elements that form flexible garments such as chain mail armours. Traditionally, the mechanical properties of these materials were considered fixed. However, recent research has revealed their mechanical properties may be varied. Notably, studies have demonstrated that applying vacuum pressure between layers of 3D-printed chain mails enclosed in a bag induces particle and layer jamming of the elements, thereby affecting the material's bending modulus. This arises from both compressive frictional forces and the complex geometrical interlocking of the rigid elements. This paper presents a comprehensive set of experimental tests for the characterisation of the stiffness and damping properties with respect to the type and number of fabrics and with respect to the vacuum pressure. More specifically, the study examines experimentally the changes in static properties in response to vacuum pressure changes evaluated on a four- and six-point bending setups. The outcome of this measurement campaign is then reported into the Ashby diagrams to compare the mechanical properties of the in-vacuum structured fabrics with those of classical materials. The potential applications of this research include the development of lightweight adaptive and semi-active vibration mitigation devices.

Keywords Smart materials · Tuneable · Vacuum · Bending test

1 Introduction

Conventional knitted fabrics are inherently compliant due to their composition of pliable threads. Structured fabrics instead are composed by a network of structural rigid elements linked together in an established pattern to form a flexible mesh. For instance, chain mail armours, which have been used by armies for over 20 centuries, are structured fabrics obtained by linking metal rings. Several patterns of linked rings have been known since ancient times, with the most common being the 4-to-1 pattern (where each ring is linked with four others) using both riveted and solid rings. Thanks to 3D-printing technology, nowadays it is possible to create structured fabrics with particles formed as 3D structures, constructed from connecting trusses, designed to reduce the overall density and enhance contacts between elements. Emerging 3D-printing technologies are processes whereby parts or components are directly built from a solid model using a heat source and filler material, which includes among many, fusion deposition modelling and selective laser sintering [1]. 3D-printing technology has the benefits of being simple, adaptable, cheap, fast, efficient, durable, and suitable for the rapid design and fabrication of irregular and complex shapes [2]. These new manufacturing techniques enable innovative and more efficient composite designs, which have numerous applications, including in the aeronautic sector [3]. Additive manufacturing can also be used to create smart multifunctional components by directly incorporating electrical connections and components during the manufacturing process [4]. Moreover, the ability to produce pieces of textiles without the constraints placed by conventional manufacturing processes such as knitting, and weaving are of great advantage to fashion designers as well as designers of functional wearables. By printing rigid individual links that can be assembled into a wearable piece, designers have created fashion pieces [5]. Structured fabrics, such as woven sheets or chain mail armours, show a large range of characteristics, such as high impact resistance, thermal regulation, electrical conductivity, which can be achieved thanks to both the constitutive materials and their

✉ E. Rustighi
emiliano.rustighi@unitn.it

[1] Dipartimento Ingegneria Industriale, Università degli Studi di Trento, Trento, Italy

[2] Dipartimento Politecnico di Ingegneria e Architettura, Università degli Studi di Udine, Udine, Italy

[3] ProM Facility, Trentino Sviluppo S.P.A., Rovereto, Italy

geometry [6, 7]. Nevertheless, once produced, the properties of the fabrics typically remain fixed.

Wang et al. [8] presented a new smart material, the tuneable structured fabric (TSF), consisting of 3-dimensional truss-unit particles arranged into layered chain mails and placed into a vacuum bag. When vacuum pressure is exerted, the particles jam with each other and, it has been shown that, even with a small external pressure (about 93 kPa), the material becomes more than 25 times stiffer than in the unpressurised configuration. It was also shown that when several layers are overlapped, a layer jamming influences the response as well as the particle jamming. The research study presented in Ref. [8] aimed at providing lightweight, tuneable, and adaptive fabrics, for applications in wearable exoskeletons, haptic architectures, and reconfigurable medical supports. Recently, Rustighi et al. [9] characterised the TSF from a vibrational point of view studying experimentally the vibration response of beam-like specimens formed by single-layer or double-layer TSF encompassing spherical-octahedra, octahedra and cubes truss-like rigid elements. They conducted both quasi-static and dynamic analyses of the bending stiffness and energy dissipation of these specimens. Specimens constructed with cubic elements exhibited the highest bending stiffness and fundamental resonance frequency. They showed that while the bending stiffness is strongly dependent on confinement pressure, the level of vacuum had little effect on the loss factors.

A promising area for exploration in the use of TSF could be the creation of devices aimed at mitigating vibrations. For instance, tuneable devices for the mitigation of vibrations have been studied using other smart materials such as shape memory alloys [10], magnetorheological elastomers [11], electro-magnetic transducers [12] and piezoelectric patch [13–16]. Although such devices have demonstrated their effectiveness, their range or speed of adaptation has shown some limitations. The use of TSF seems to promise a large and quick range of adaptation. However, no research on the use of structured fabric for the realisation of vibration and noise mitigation devices has ever been done. More recently, vibration mitigation devices have been discussed which use a confining pressure on granular material [17, 18]. Linear and torsional vibration absorbers have been designed and tested where variable dissipative properties were obtained by changing the confining pressure of vacuum-packed particles. No tuning, or change of the stiffness, was obtained by these devices. In the aeronautic sector, advanced smart materials are proposed to achieve adaptive morphing shapes, leading to performance improvements, such as through the use of inflatable winglets [19].

The effect of the confining pressure and the reversible and gradual switch between soft and rigid states has been studied extensively for disordered materials [20–24] where jamming has been indicated as the phenomenon responsible for this behaviour. A broad class of disordered materials including foams, glassy molecular systems, colloids and granular materials exhibit the formation of jammed states. A jammed system resists small stresses without deforming irreversibly, whereas an unjammed system flows under any applied stress. Jamming is a phase transition that depends mainly on confining pressure and shear stress. In particular, when pressure is increased, the number of contact points between particles increases, thus reducing the effective degrees of freedom of the particles. When the number of contact points is large enough to reach an isostatic condition, the material is at the jamming transition point. From this jamming transition point, any rise in confining pressure causes an increase in the material stiffness and in the yielding shear strength. In fact, unjamming or plastic flow can be induced by decreasing the confining pressure or by increasing the shear stress. The boundary between unjammed and jammed regions is the yield stress line. This kind of transition allows the structure to change reversibly from a solid (jammed) state to a fluid state.

As it happens for granular media, so structured fabrics react to a confining pressure by jamming. However, the jamming of structured fabrics differs from the jamming of granular media. Granular media is a fully disordered material, while structured fabrics have a loose lattice structure. In fact, structured fabrics are made of particles with the same geometry and dimensions and interconnected in an orderly manner. During the compaction, imposed by a confining pressure, the order in the loose lattice structure is somehow maintained giving origin to a partially ordered structure. This may make the behaviour of the material more predictable and able to be engineered. Another difference is due to the fact that, when the particles of the structured fabric are pulled together by a vacuum pressure, their contact occurs via concave surfaces which permit larger contact surfaces in comparison to the convex contact areas in granular materials. Structured fabrics have also the advantage of their particles being interlocked. Locking acts on the tensile forces since the particles are interconnected and cannot be divided. This mechanism is important especially when the vacuum fails since it gives the structure a tensile strength that would not be possible in the case of loose grains. Finally, sheets of structured fabrics respond to both the particle- and layer-jamming phenomena [8, 9].

This paper investigates the mechanical response of TSFs when subject to variable vacuum pressures. The study is carried out on interwoven fabrics encompassing rigid truss-like elements made with three different geometries, namely octahedra, octahedral spheres and cubes. The TSFs have been obtained by inserting the structured fabric in airtight bags. When pressure is exerted at their boundaries, the particles jam and the structured fabric bending stiffness shows to be largely dependent on the confining pressure. Bending

tests are presented to characterise how the properties of the material vary according to the degree of vacuum generated. Both single- and double-layer configurations have been considered. Using multiple separate layers allows for the construction of thicker and, therefore, stiffer structures, which can easily adapt to non-smooth surfaces. In addition, tunability through confinement pressure on multiple-layer TSF will benefit not only from particle jamming but also from layer jamming. Finally, TSF properties have been compared to other materials by inserting them in the Ashby plots for material selection.

2 In Vacuum Structured Fabrics: Design, Fabrication, and Packaging

The design of tuneable fabrics has been inspired by the mediaeval chain mail [5] which are structured fabrics where elemental rigid truss structures are interconnected to each other so to create flexible macro-materials. Several structured fabrics can be designed, and they are distinguished by the geometry of the rigid basic element and by the lattice organisation of such elements. In this study, three geometries of the basic truss-unit particle have been considered, namely octahedra, octahedral spheres, and cubes. The elements are organised in a lattice array interconnecting at 90°. Figure 1a, b, c shows the structured fabrics' specimens manufactured for this study. Octahedra have been chosen as benchmark structures since they are able to pack in a someway ordered manner when subjected to a confining pressure. Octahedral spheres have been compared to the octahedral since they present a smoother outer geometry which should have a different effect on the layer jamming compared to the particle jamming. Cubes are also chosen to take into consideration a truss-unit particle with less packing order. The dimension of each elemental cell is around 1 cm in size. These can be considered as connected truss-like structures with a circular cross-section of about 1.5 mm in diameter. Table 1 shows the rendering of the basic cell and its connections to other elements for the three fabrics which have been manufactured and studied in this paper. Table 1 also gives the main dimensions and weight of the prototyped structured fabrics considered in this paper.

Each element in the structured fabric is a closed truss structure which has been manufactured and interconnected thanks to a process of rapid prototyping, hence there are no discontinuities in the elements due to welding, glueing or plastic deformation. For this study, the structured fabrics have been manufactured by an HP multi-jet fusion (MJF) printer. MJF technology has become one of the most commonly used 3D-printing methods to obtain highly accurate and durable parts. It is a technology ideal not only for functional prototypes, but also for the production of very complex geometries, not achievable with other additive manufacturing methods. Compared to its powder bed fusion counterparts such as selective laser sintering (SLS), MJF prints are more cost effective on a large scale. MJF-printed parts are widely used both for prototypes and end-use components. Since MJF 3D printing belongs to the additive manufacturing technology that uses powder bed fusion, it does not need support structures and complex post processing operations. During printing, all empty spaces are filled with unused powder, making MJF prints self-supporting. MJF allows for parts consolidation and very complex and

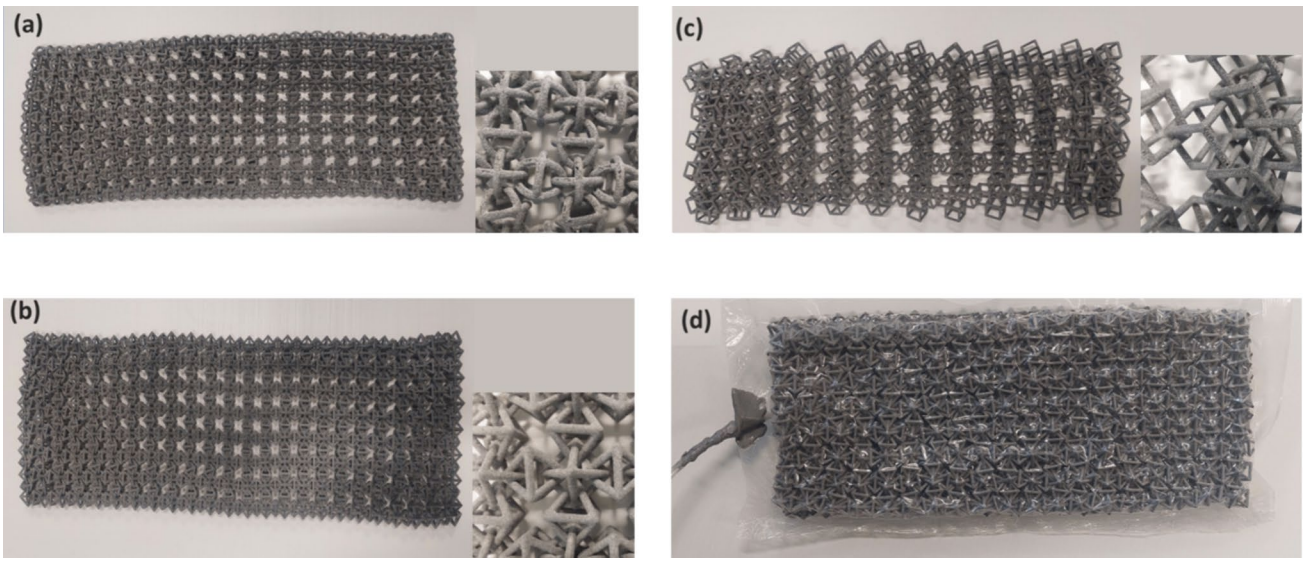

Fig. 1 Structured fabrics with **a** spherical, **b** tetrahedral, **c** cubic grains. **d** Fabric wrapped in an airtight plastic bag

Table 1 Global envelope dimension and weight of the prototyped structured fabrics

Element type	Geometry	Width (mm)	Length (mm)	Thickness (mm)	Mass (g)
Spheres		100	210	10	49
Octahedra	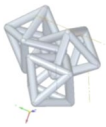	110	240	15	62
Cubes	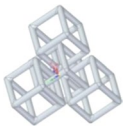	110	190	15	39

interconnected geometries, which is generally a problem using alternative technologies such as fused deposition modelling or stereolithography. With MJF, it is possible to print a given component through fusion of ultra-thin layers (on the order of 80 μ m). This results in low porosity and high density that allow the printed component to have excellent resolution and good dimensional accuracy. Hence, the surface finish of parts printed in MJF is very good. The MJF 3D-printing process results in highly isotropic parts with high strength and homogeneity along all directions.

The structured fabrics have been manufactured in Nylon PA12. The material has a nominal powder melting point of 187°, a nominal tensile strength of 48 MPa and a nominal Young's modulus of 1800 MPa, as provided by the supplier. The printer used to manufacture the fabrics was a HP jet fusion 3D 4200, which has a build volume of $380 \times 284 \times 380$ mm. The printing velocity in height is 23.75 mm/h. Then, the build needs to cool down in a slow and controlled manner: this phase is the longest and most critical to achieve the maximum quality and dimensional stability. For every hour of printing, 3 h of cooling is required: in less than 3 days, a full job is ready to be unpacked and processed to obtain the final parts.

The 3D-printed structured fabrics have then been assembled inside a vacuum bag in order to obtain TSFs. In this study, vacuum bags (commonly used for food preservation) have been used to wrap one or two layers of the prototyped structured fabrics. The sides of the bag have been adapted to the structured fabric dimension and sealed by the application of a hot iron. Where the application of the hot iron was not possible, butyl sealing tape has been used to seal the open sides and connection points. A diaphragm vacuum pump (KNF NEUBERGER UN726 TTP) has been connected to the vacuum bag via a pneumatic pipe, two pneumatic valves and an analogue vacuum metre. The additional weight of the butyl strips has been estimated to be 6 g. Figure 1d shows a preliminary assembly in which the pneumatic pipe was inserted into the bag by the opening side and sealed with butyl sealing tape.

3 Bending Stiffness from Quasi-static Four-Point Tests

Four-point bending tests were implemented to evaluate the bending stiffness of the TSF and its variation with type of elemental structure and confinement pressure. Figure 2a shows the test carried out on a prototyped TSF. The four-points bending test is characterised by four loading points as illustrated in Fig. 2a. This test configuration was chosen since it allows to measure the bending stiffness in the material specimen while reducing the effect of shear. The samples were tested in a four-point bending setup using a Tinius Olsen H10KT universal testing machine equipped with a 1 kN load cell and operating at a 1 mm/s crosshead displacement rate. The distance between the two upper points was $\ell = 80$ mm, while the lower points were separated by $L = 160$ mm. The test was composed by three cycles of loading and unloading imposing a displacement of 10 mm to the upper points. Confining pressures of 20, 40, 60 and 80 kPa have been considered. Tests have been conducted with one or two layers of structured fabric inside the vacuum bag.

A linear fitting on the measurements that minimises the root-mean-square-error allows to obtain an estimate of the stiffness of the specimen, k_{4p}, which can be related to the bending stiffness, EI, by

$$k_{4p} = \frac{24EI}{(L-\ell)^2\left(\frac{L}{2}+\ell\right)} \tag{1}$$

where L is the distance between the outer supports, ℓ is the distance between the inner supports, E is the effective

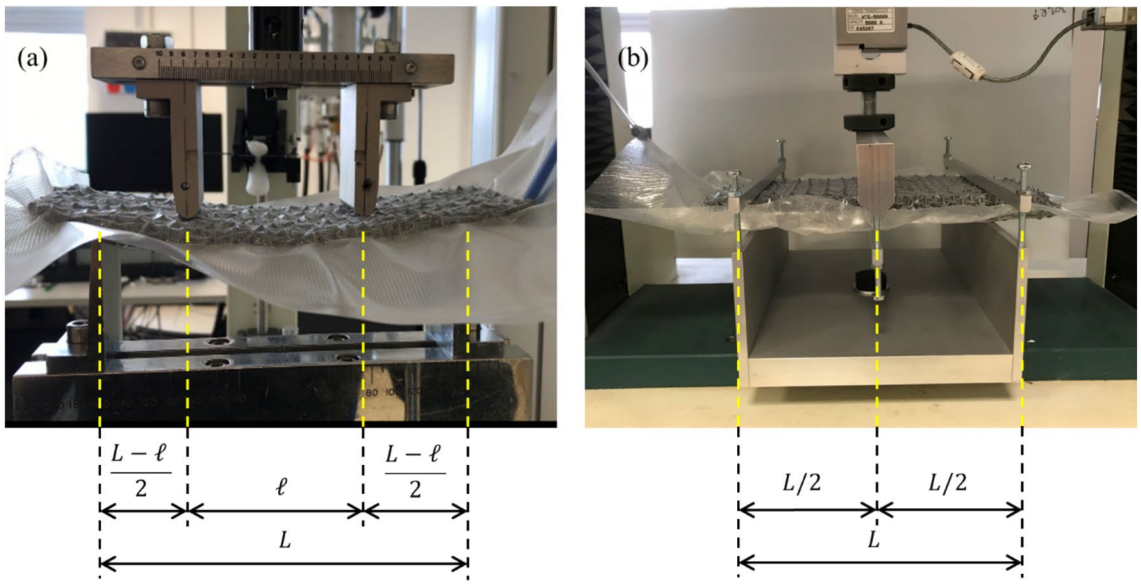

Fig. 2 Bending stiffness and hysteresis characterisation by **a** four-point and **b** six-points tests

Young's modulus of elasticity of the material, and $I = \frac{bh^3}{12}$ is the cross-section second moment of area, where b and h are the width and thickness of the specimen.

Figure 3 shows the force–deflection curve for TSFs obtained with a single and double layer inserted in the vacuum bag. The curves are relative to the second loading and unloading of the specimens. In fact, it was observed a lower stiffness in the first loading curve with respect to the second one. This is probably due to the geometric reorganisation of the fabric solid elements. The successive loading and unloading curves instead are very similar to the previous ones. This led to the conclusion that one loading/unloading cycle was sufficient for all the elements to reach a final equilibrium in the contact positions. It is also evident that while the loading curve is nearly linear, the unloading curve exhibits pronounced nonlinear trend. This may be due to the reduction in the number of contacts during unloading,

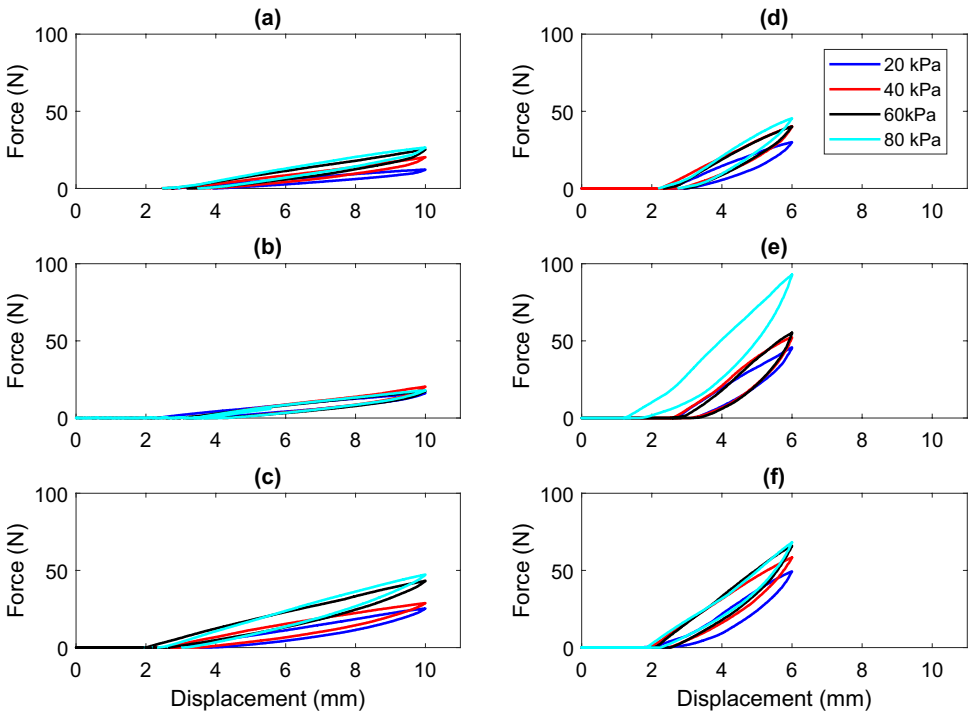

Fig. 3 Measured force–displacement loading curve for octahedral spheres (**a, d**), octahedra (**b, e**) and cubes (**c, f**) for a single (**a, b, c**) and double (**d, e, f**) layers

but further experimental and numerical investigations are needed to clarify the reasons for this behaviour. Figure 3d, e, f shows the loading curve in the case of two layers overlapped and inserted into the bag. The double-layer configuration greatly increases the stiffness. This is partly due to the increase of the second moment of area and partly to the extra entanglement between the two overlapped layers (layer jamming).

The loading curves show a linear trend. It is possible to interpolate a linear curve and obtain the stiffness of specimen and derive from this the bending stiffness EI, which has been reported in Fig. 4. The unloading curves are instead characterised by a variable tangent stiffness. This asymmetric behaviour is probably caused by discontinuous frictional forces at each contact point. Figure 4 shows how the interpolated bending stiffness of the TSF varies with the confinement pressure. The data are obtained from the second loading curve since the first one settles the jamming of the basic elements into the layer. For the single-layer configuration, the cubes show the largest value of stiffness and the largest increment of bending stiffness (about 110% from 20 to 80 kPa). Octahedral spheres show lower values of bending stiffness but a similar value of increment (about 110% from 20 to 80 kPa). Very interestingly, the octahedra show almost no increment in bending stiffness with the confining pressure (about 30% from 20 to 80 kPa). It looks like particle jamming is less effective for this lattice structure. In fact, they reach a saturation or plateau at a very low pressure, probably below 20 kPa. The stiffest fabric is that with cubic elements, which results into a comparatively thicker layer of 15 mm, as reported in Table 1.

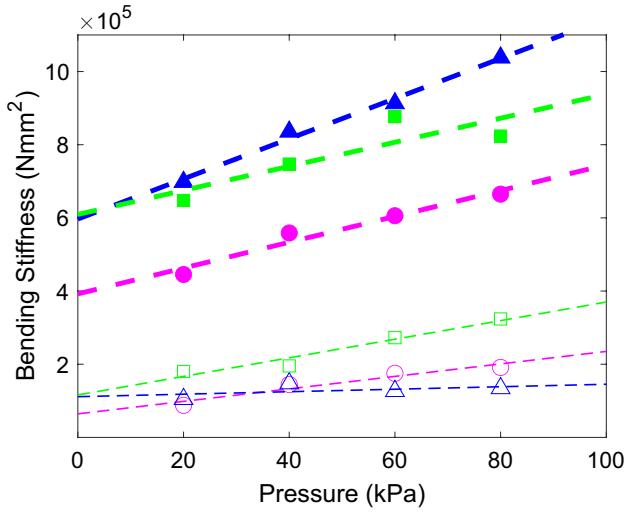

Fig. 4 Measured bending stiffness of the tuneable structured fabrics assembled with one (thin lines with empty markers) or two overlapped layers (thick lines with filled markers). The points represent the measured data while the line shows the interpolated value. Magenta circles for octahedral spheres, blue triangles for octahedra and green squares for cubes

For the double-layer configuration, the octahedral elements show the largest increment of bending stiffness from single to double layer and with confinement pressure (about 48% from 20 to 80 kPa). This is surprising since the single layer showed almost no dependency on the confinement pressure. This indicates that the layers jamming for this cell type plays a fundamental role. Octahedral spheres show a reasonable increment of bending stiffness from single to double layer and also an increased slope in the confinement pressure dependence. The cubes fabric shows the smallest increment with confinement pressure (about 29% from 20 to 80 kPa). Octahedra and cubes fabrics show the largest bending stiffnesses.

4 Hysteresis Cycle from Quasi-static Six-point Tests

In order to study the material losses, hence the loss factor of the material, the materials have been subjected to closed stress cycle in a six-point bending test. Hysteresis loops that represent the energy lost in the cycle have been obtained. The six-point bending test configuration allows to push and pull the specimen during the same testing cycle in order to record hysteresis loops and hence evaluate the energy dissipated per cycle. From these measurements, the loss factor can be evaluated [25]. Figure 2b shows the test setup. The rig was realised using purposedly manufactured clamps. The three pincers-like clamps were designed in such a way to constrain only the transverse displacement of the beam allowing thus free rotation. Therefore, as depicted in Fig. 2b, the beam specimen is simply supported in proximity of the two ends and undergoes an imposed transverse displacement w in the middle span. The six-point bending test is indeed characterised by three bilateral loading points as illustrated in Fig. 2b. The distance between the two farther apart points was $L = 160$ mm. The test was composed by three cycles of loading and unloading imposing a displacement of 0.5 mm to the upper points to largely stay in the linear range. The frequencies tested have been 6 Hz, 3 Hz and 1.5 Hz. Deformation velocities peaked at about 18.8 mm/s, 9.4 mm/s and 4.7 mm/s, respectively.

Several models have been proposed for describing the energy dissipation mechanism or damping, which is responsible of the decaying of the oscillatory motion. Viscous damping, velocity-squared damping, Coulomb damping (dry friction), hysteretic damping (structural material damping) and sound radiation damping are models commonly adopted to describe the energy dissipation in vibrating structures. In particular, hysteretic or structural damping is used to characterise material losses in metals and viscoelastic materials. Structural

damping is attributed to the hysteresis phenomenon associated with cyclic stress in elastic material. The loss factor, η, is the material properties which is given by the ratio between the loss modulus (imaginary part of the complex modulus of elasticity) and the storage modulus or Young's modulus. Hence, we can define a complex modulus of elasticity of the material as $E^* = E(1 + \eta \mathrm{i})$ where $\mathrm{i} = \sqrt{-1}$. A structural damping model has been used to take into account the internal damping of materials. The energy loss per cycle of stress is equal to the area inside the hysteresis loop. Assuming an hysteretic damping model, the material loss factor value was calculated with respect to the total energy dissipated in a harmonic cycle ΔE_c, which is given by the area of the hysteresis loop, and with respect to the peak strain potential energy U_m, which is given by the product of the peak force and peak displacement, such that [25].

$$\eta = \frac{1}{2\pi} \frac{\Delta E_c}{U_m} \tag{2}$$

Hysteresis cycles are used to measure the damping characteristics of the material under investigation. Figure 5 shows how the hysteresis loop change with confining pressure and lattice structural element. The area of the loop is an indication of the energy dissipated in each cycle while the slope of the curves is an indication of the stiffness in the specimen. It is clear from Fig. 5 that the confining pressure has negligible effect on the damping of the material. Further tests at different frequencies have also shown minor changes in the loss factor with frequency and no change with pressure. Figure 6 shows the extrapolated values of loss factor. The loss factor does not seem to change much from single to double layer. Although the dissipated energy per cycle, i.e. the hysteresis loop area, increases from single to double layer, the loss factor does not change significantly, because of the consequent increase in stiffness.

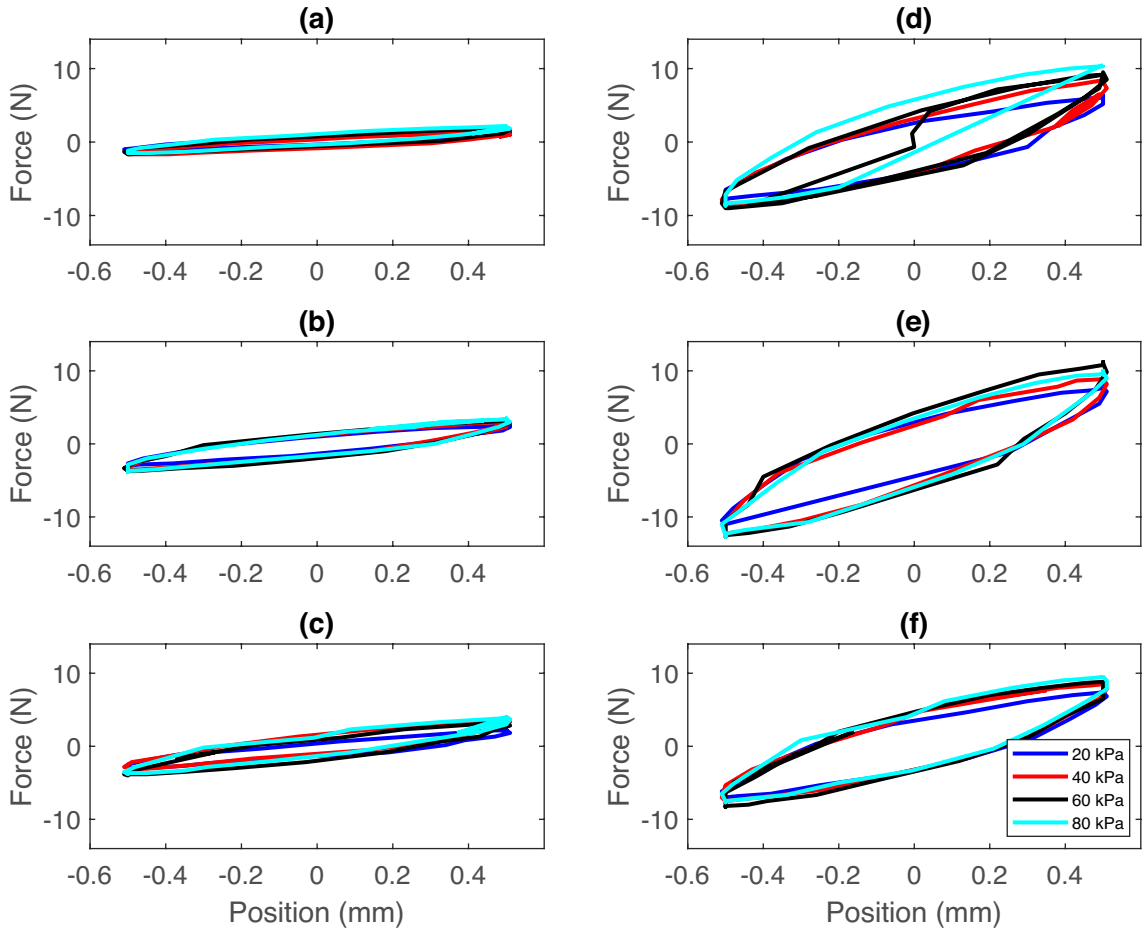

Fig. 5 Hysteretic response at 6 Hz for octahedral spheres (**a, d**), octahedra (**b, e**) and cubes (**c, f**) for a single (**a, b, c**) and double (**d, e, f**) layers

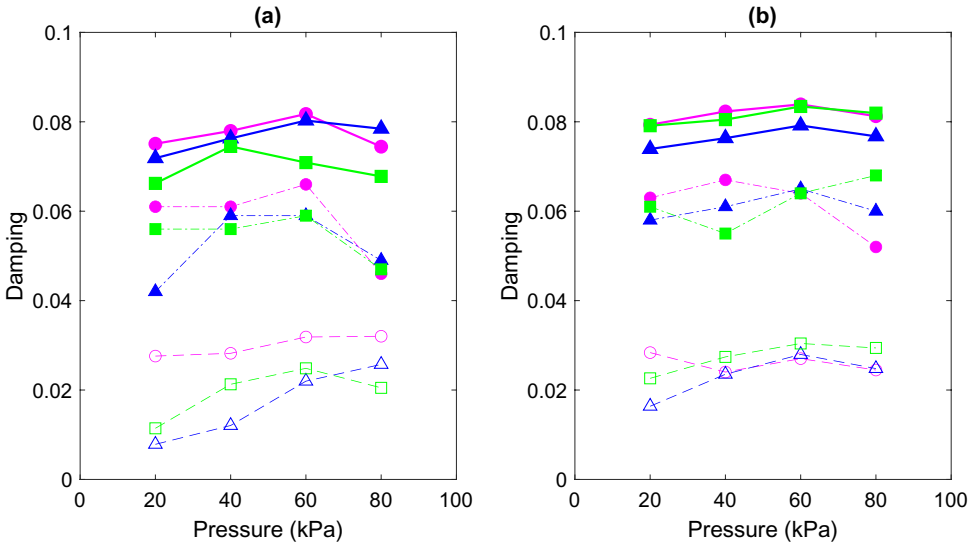

Fig. 6 Structural loss factor of the tuneable structured fabrics assembled with one **a** or two **b** overlapped layers evaluated from data obtained at 1.5 Hz (dashed lines), 3 Hz (dot-dash lines) and 6 Hz (continuous lines). The points represent the measured data. Magenta circles for octahedral spheres, blue triangles for octahedra and green squares for cubes

5 Material Evaluation

The TSF can be evaluated and compared to other traditional materials thanks to the Ashby material maps shown in Fig. 7. With a Young's modulus and density akin to high-performance foams, TSFs share similarities with foams, metals, and ceramics in their Young's modulus to density ratio. In addition, TSFs show large values of loss factors for appreciable values of the Young's modulus. However, TSF offers the distinct advantage of tuneable stiffness, allowing for the design of devices with precisely tailored stiffness properties. This versatility positions TSF as a promising material for the development of vibration and noise mitigation devices, supplementing existing foam applications with its unique tuneability.

6 Future Research

Future research on TSF will focus on its application as a device for vibration and noise mitigation. In addition, future studies will develop a model of the system to enable numerical investigations. This will facilitate parametric studies and help derive optimised shapes or design guidelines. The numerical analysis will encompass both homogenisation models, finite-element models, and discrete-element models.

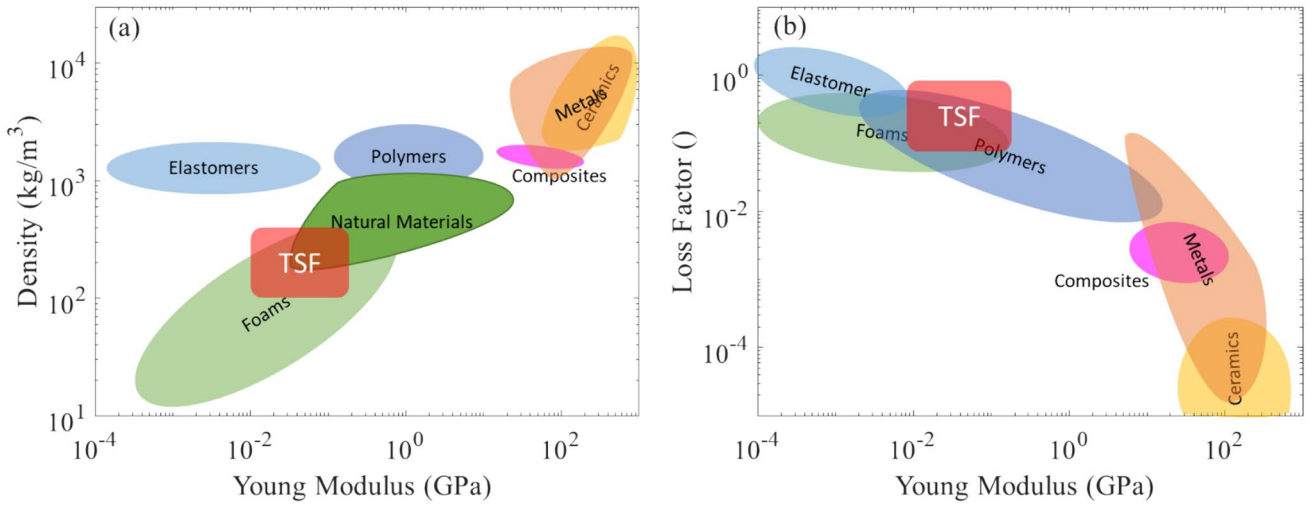

Fig. 7 Ashby diagrams including in-vacuo tuneable structured fabric (TSF): **a** density vs Young's modulus and **b** loss factor vs Young's modulus

7 Conclusions

This study delves into the static characteristics of TSF, a novel form of metamaterial comprising 3D-printed structured fabric encased within a vacuum pressure-controlled bag. Analysis of force–displacement curves reveals an initially linear regime governed by the elastic behaviour of the jammed granular structure, with a slight nonlinear response observed as the confinement pressure increases, likely linked to local particle rearrangements. Stiffness correlates directly with the number of contacts, resulting in increased rigidity under higher vacuum levels due to greater contact points. Employing a double-layer configuration significantly enhances the stiffness and the tuneable range. Confinement pressure impacts minimally on the loss factor.

Author contributions E.R., P.G. and S.B. assembled the tuneable strutured fabrics, carried the experimental campaogn out, wrote the main manuscript test and prepared the figures. M.P. and C.M. rendered and manufactured the fabrics. All authors reviewed the manuscript.

Funding Open access funding provided by Università degli Studi di Trento within the CRUI-CARE Agreement. This work was funded by the European Union under NextGeneration EU. PRIN 2022 Prot. n. 20223X5S37_001.

Data availability Data sets generated during the current study are available from the corresponding author on reasonable request.

Declarations

Conflict of interest The authors declare no competing interests.

References

1. Sahasrabudhe, H., Bose, S., Bandyopadhyay, A.: Chapter 17—laser-based additive manufacturing processes. In: Lawrence, J. (ed.) Advances in laser materials processing, pp. 507–539. Woodhead Publishing Series in Welding and Other Joining Technologies Woodhead Publishing, Sawston (2018)
2. Chatterjee, K., Ghosh, T.K.: 3d printing of textiles: potential roadmap to printing with fibers. Adv. Mater. **32**(4), 1902086 (2020)
3. Catapano, A., Montemurro, M., Balcou, J.A., Panettieri, E.: Rapid prototyping of variable angle-tow composites. Aerotec. Missili Spaz. **98**, 257–271 (2019)
4. Graterol Nisi, G., Eugeni, M., Cardini, V., Atek, S., Pollice, L., Gaudenzi, P.: Basic technology for smart multifunctional components with embedded electronics using fused filament fabrication. Aerotec. Missili. Spaz. **98**, 159–172 (2019)
5. Bloomfield, M., Borstrock, S.: Modeclix. The additively manufactured adaptable textile. Mater. Today Commun. **16**, 212–216 (2018)
6. Chen, X., Taylor, L.W., Tsai, L.-J.: An overview on fabrication of three-dimensional woven textile preforms for composites. Text. Res. J. **81**(9), 932–944 (2011)
7. Tabiei, A., Nilakantan, G.: Ballistic impact of dry woven fabric composites: a review. Appl. Mech. Rev. (2008). https://doi.org/10.1115/1.2821711
8. Wang, Y., Li, L., Hofmann, D., Andrade, J.E., Daraio, C.: Structured fabrics with tunable mechanical properties. Nature **596**(7871), 238–243 (2021)
9. Rustighi, E., Gardonio, P., Baldini, S., Malacarne, C., Perini, M.: Vibration response of in-vacuo tuneable structured fabrics. J. Vibrat. Control. **1**(1), 1–20 (2024)
10. Rustighi, E., Brennan, M., Mace, B.: A shape memory alloy adaptive tuned vibration absorber: design and implementation. Smart Mater. Struct. **14**(1), 19 (2004)
11. Rustighi, E., Ledezma-Ramirez, D.F., Tapia-Gonzalez, P.E., Ferguson, N., Zakaria, A.: Modelling and experimental characterisation of a compressional adaptive magnetorheological elastomer isolator. J. Vibrat. Control. **28**(21–22), 3093–107 (2021)
12. Gardonio, P., Casagrande, D.: Shunted piezoelectric patch vibration absorber on two-dimensional thin structures: tuning considerations. J. Sound Vib. **395**, 26–47 (2017)
13. Gardonio, P., Turco, E., Kras, A., Dal Bo, L., Casagrande, D.: Semi-active vibration control unit tuned to maximise electric power dissipation. J. Sound Vib. **499**, 116000 (2021)
14. Iannelli, P., Angeletti, F., Gasbarri, P.: Model-based FDI applied to a piezoelectric active vibration suppression system for smart flexible spacecraft. Aerotec. Missili Spaz. **100**, 147–160 (2021)
15. Gardonio, P., Konda Rodrigues, G., Dal Bo, L., Turco, E.: Extremum seeking online tuning of a piezoelectric vibration absorber based on the maximisation of the shunt electric power absorption. Mech. Syst. Signal Proc. **176**, 109171 (2022)
16. Konda Rodrigues, G., Gardonio, P., Dal Bo, L., Turco, E.: Piezoelectric patch vibration control unit connected to a self-tuning RL-shunt set to maximise electric power absorption. J. Sound Vibrat. **536**, 117154 (2022)
17. Zalewski, R., Bartkowski, P.: Prototype of a controllable damper based on granular materials subjected to partial vacuum. MATEC Web Conf. **254**, 05009 (2019)
18. Rodak, D., Zalewski, R.: Innovative controllable torsional damper based on vacuum packed particles. Materials **13**(19), 4356 (2020)
19. De Fenza, A., D'Orazio, D., Barile, M., Lecce, L.: Development of finite element model for morphing inflatable winglet. Aerotec. Missili Spaz. **94**, 124–132 (2015)
20. Behringer, R.P., Chakraborty, B.: The physics of jamming for granular materials: a review. Rep. Prog. Phys. **82**(1), 012601 (2018)
21. Boonen, R., Sas, P., "Modified smith compensation for feedback active noise control in ducts," in Proceedings of the 2001 International Congress and Exhibition on Noise Control Engineering, The Hague, The Netherlands. 619–624 (2001)
22. Levine, D. "Jamming and the statics of granular materials." Jamming and Rheology: Constrained Dynamics on Microscopic and Macroscopic Scales. 9 (2001).
23. Liu, A.J., Nagel, S.R.: Jamming and rheology: constrained dynamics on microscopic and macroscopic scales. CRC Press, Boca Raton (2001)

24. Liu, A.J., Nagel, S.R.: The jamming transition and the marginally jammed solid. Annu. Rev. Condens. Matter Phys. **1**(1), 347–369 (2010)
25. Jones, D.I.G.: Handbook of viscoelastic vibration damping. John Wiley & Sons, Hoboken (2001)